 CMES, vol.88, no.1, pp.1-16, 2012

Numerical Simulation of Plane Crack Using Hermite Cubic Spline Wavelet

Jiawei Xiang[1,2], Yanxue Wang[3], Zhansi Jiang[3]
Jiangqi Long[1] and Guang Ma[1]

Abstract: Two-dimensional wavelet-based numerical approximation using Hermite cubic spline wavelet on the interval (HCSWI) is proposed to solve stress intensity factors (SIFs) of plate structures. The good localization property of wavelets is used to approximate displacement fields by multi-scale bases of HCSWI. Example computations are performed for plates with a central crack and double edge cracks. The numerical results prove that, compared with the conventional finite element method and the analytical solutions, the new procedure are efficient in both its accuracy and its reduction of degree of freedoms (DOFs).

Keywords: Plate structures; Stress intensity factors; HCSWI; Wavelet numerical method

1 Introduction

Crack propagation behavior is a major issue in a variety of structures of industries. Aerospace structures, gas turbine blade, pressure vessels, pipelines, and wind turbine blades are obvious examples where failure could lead to catastrophic consequences and loss of life. The solution of stress intensity factors (SIFs) involves a well-known mathematical difficulty. Among calculation algorithms in problems of fracture mechanics, finite element analysis (FEA) is the most commonly used method [Tada et al. (2000)]. Recently, many numerical methods were proposed to efficiently calculate SIFs. Wearing et al. [Wearing and Ahmadi-Brooghani (1999)] presented a boundary element method to analyze two-dimensional crack problems. Giner et al. proposed an extended finite element method (X-FEM) to solve crack problems and further developed an implementation of the X-FEM into the commercial FEA software Abaqus [Giner et al. (2009)]. In the above mentioned methods,

[1] College of Mechanical Engineering, Wenzhou University, Wenzhou, 325035, P.R.China.
[2] Corresponding author: Jiawei Xiang. E-mail: wxw8627@163.com
[3] School of Mechanical and Electrical Engineering, Guilin University of Electronic Technology, Guilin, 541004, P.R.China.

the efficiency and precision are key issues to overcome the large numerical error caused by crack singularity. Adaptive FEM is also an important technique to obtain more accurate values of SIFs. Kpegba et al. proposed a hybrid method to combine the two independent classical meshes to improve the precision of traditional FEA [Kpegba and Ottavy (1996)].

Wavelet numerical method was proposed to solve partial differential equations (PDEs) [Diaz et al. (2009); Vampa et al. (2010); Ma et al. (2003); Chen et al. (2009); Wang et al. (2010, 2011); He et al. (2007); Xiang et al. (2009a, 2007)]. Hermite cubic spline wavelet on the interval (HCSWI) is the new wavelet bases constructed by Jia and Liu [Jia and Liu (2006); Jia (2009)]. Xiang et al. employed HCSWI to analyze Possion equation [Xiang et al. (2009b)]. The advantage of HCSWI wavelet-based numerical method is the decoupling of multi-scaling approximation equations [Xiang et al. (2009b)].

In the present work, a new wavelet numerical method using HCSWI is proposed to calculate SIFs of plate structures. Two examples of plates with a central crack and double edge cracks are investigated. It notes that the extension of the present method to other classes of structures with cracks is possibly.

2 The wavelet bases of HCSWI

In this section, we give a brief description of HCSWI. One-dimensional multi-resolution analysis (MRA) of HCSWI is given by Jia and Liu [Jia and Liu (2006)]. The scaling functions $\phi_{1,k}$ (scale=1 and k=1, 2, 3, 4) are defined by

$$\begin{cases} \phi_{1,1}(x) := \sqrt{\frac{5}{24}}\phi_1(2x-1) \\ \phi_{1,2}(x) := \sqrt{\frac{15}{4}}\phi_2(2x) \\ \phi_{1,3}(x) := \sqrt{\frac{15}{8}}\phi_2(2x-1) \\ \phi_{1,4}(x) := \sqrt{\frac{15}{4}}\phi_2(2x-2) \end{cases} \tag{1}$$

and the wavelets $\psi_{j,k}$ (scale=j and k=1, 2, …, 2^{j+1})are

$$\begin{cases} \psi_{j,k}(x) := \frac{2^{-j/2}}{\sqrt{729.6}}\psi_1\left(2^j x - \frac{k}{2}\right) & \text{for } k = 2,4,\ldots,2^{j+1}-2, \\ \psi_{j,k}(x) := \frac{2^{-j/2}}{\sqrt{153.6}}\psi_2\left(2^j x - \frac{k-1}{2}\right) & \text{for } k = 3,\ldots,2^{j+1}-1, \\ \psi_{j,1}(x) := \frac{2^{-j/2}}{\sqrt{76.8}}\psi_2\left(2^j x\right), \\ \psi_{j,2^{j+1}}(x) := \frac{2^{-j/2}}{\sqrt{76.8}}\psi_2\left(2^j x - 2^j\right), \end{cases} \tag{2}$$

in which ϕ_1 and ϕ_2 be the cubic splines supported on the interval [-1, 1] as

$$\phi_1(x) := \begin{cases} (x+1)^2(1-2x) & \text{for } x \in [-1,0] \\ (1-x)^2(1+2x) & \text{for } x \in [0,1] \\ 0 & \text{for } x \notin [-1,1] \end{cases}$$

and

$$\phi_2(x) := \begin{cases} (x+1)^2 x & \text{for } x \in [-1,0] \\ (x-1)^2 x & \text{for } x \in [0,1] \\ 0 & \text{for } x \notin [-1,1] \end{cases} \tag{3}$$

and the wavelets ψ_1 and ψ_2 are supported on the interval [-1, 1] as

$$\begin{cases} \psi_1(x) = -2\phi_1(2x+1) + 4\phi_1(2x) - 2\phi_1(2x-1) - 21\phi_2(2x+1) + 21\phi_2(2x-1) \\ \psi_2(x) = \phi_1(2x+1) - \phi_1(2x-1) + 9\phi_1(2x+1) + 12\phi_2(2x) + 9\phi_2(2x-1) \end{cases} \tag{4}$$

Hermite cubic splines ϕ_1 and ϕ_2, wavelets ψ_1 and ψ_2 are shown in Figs.1 and 2, respectively

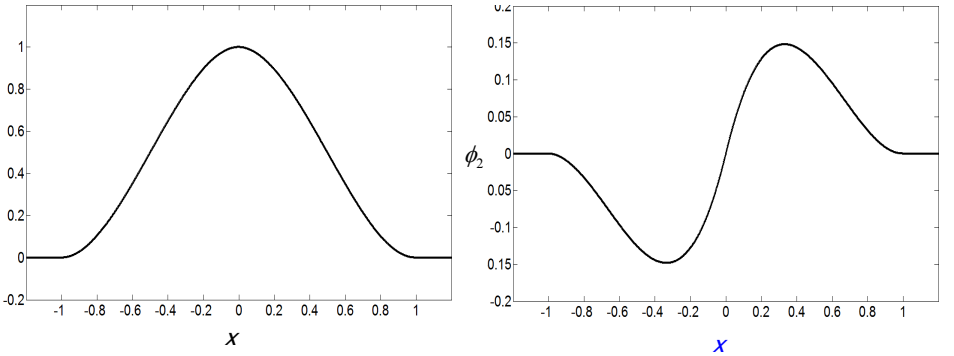

(a) Symmetric cubic spline (b) Anti-symmetric cubic spline

Figure 1: Hermite cubic splines ϕ_1 and ϕ_2

The special property of HCSWI is

$$\begin{cases} \left\langle \phi'_{1,k_1}, \psi'_{j,k_2} \right\rangle = \int_0^1 \phi'_{1,k_1} \psi'_{j,k_2} \mathrm{d}x = 0 & \text{for all } j \\ \left\langle \psi'_{j_1,k_1}, \psi'_{j_2,k_2} \right\rangle = \int_0^1 \psi'_{j_1,k_1} \psi'_{j_2,k_2} \mathrm{d}x = 0 & \text{for } j_1 \neq j_2 \end{cases} \tag{5}$$

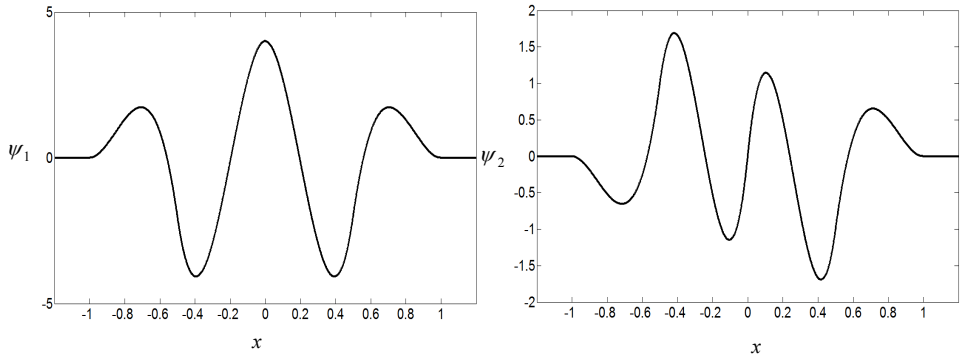

(a) Symmetric wavelet (b) Anti-symmetric wavelet

Figure 2: Wavelets ψ_1 and ψ_2

The wavelet bases in scale space V_j can be written by

$$\boldsymbol{\phi}_j = [\boldsymbol{\phi}_1, \boldsymbol{\psi}_1, \boldsymbol{\psi}_2, \cdots, \boldsymbol{\psi}_{j-1}] \tag{6}$$

where $\boldsymbol{\phi}_1 = [\phi_{1,1}, \phi_{1,2}, \phi_{1,3}, \phi_{1,4}]$ denotes scaling functions in V_1, and $\boldsymbol{\psi}_s (s = 1, 2, \cdots j-1)$ consists of the wavelet bases in wavelet space W_s, i.e., $\boldsymbol{\psi}_s = [\psi_{s,1}, \psi_{s,2}, \cdots, \psi_{s,2^{s+1}}]$. Fig. 3 shows the first derivative of $\boldsymbol{\phi}_1$ and $\boldsymbol{\psi}_1$.

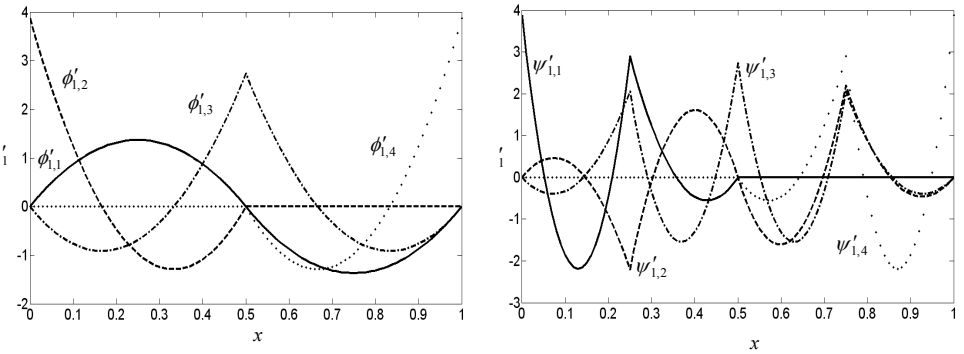

(a) The first derivative of $_1$ (b) The first derivative of $_1$

Figure 3: The first derivative of $\boldsymbol{\phi}_1$ and $\boldsymbol{\phi}_1$

To construct two-dimensional wavelet bases, tensor product of one-dimensional wavelets is a direct way [Chen et al. (2004); Zhang et al. (2010); Mallat (1999)]. Take $\boldsymbol{\phi}_2 = [\boldsymbol{\phi}_1, \boldsymbol{\psi}_1]$ for example, the two-dimensional scaling and wavelet functions

are

$$\boldsymbol{\phi}_2 \otimes \boldsymbol{\phi}_2 = [\boldsymbol{\phi}_1 \otimes \boldsymbol{\phi}_1, \boldsymbol{\phi}_1 \otimes \boldsymbol{\psi}_1, \boldsymbol{\psi}_1 \otimes \boldsymbol{\phi}_1, \boldsymbol{\psi}_1 \otimes \boldsymbol{\psi}_1] = [\boldsymbol{\phi}^1, \boldsymbol{\psi}^2, \boldsymbol{\phi}^3, \boldsymbol{\psi}^4] \tag{7}$$

where $\otimes$ is the kronecker symbol. Therefore, we obtain four functions, namely, the scaling functions $\boldsymbol{\phi}^1 = \boldsymbol{\phi}_1 \otimes \boldsymbol{\phi}_1$, wavelets$\boldsymbol{\psi}^1 = \boldsymbol{\psi}_1 \otimes \boldsymbol{\phi}_1$, $\boldsymbol{\psi}^2 = \boldsymbol{\phi}_1 \otimes \boldsymbol{\psi}_1$ and $\boldsymbol{\psi}^3 = \boldsymbol{\psi}_1 \otimes \boldsymbol{\psi}_1$, which are shown in Fig.4(a), (b), (c) and (d), respectively.

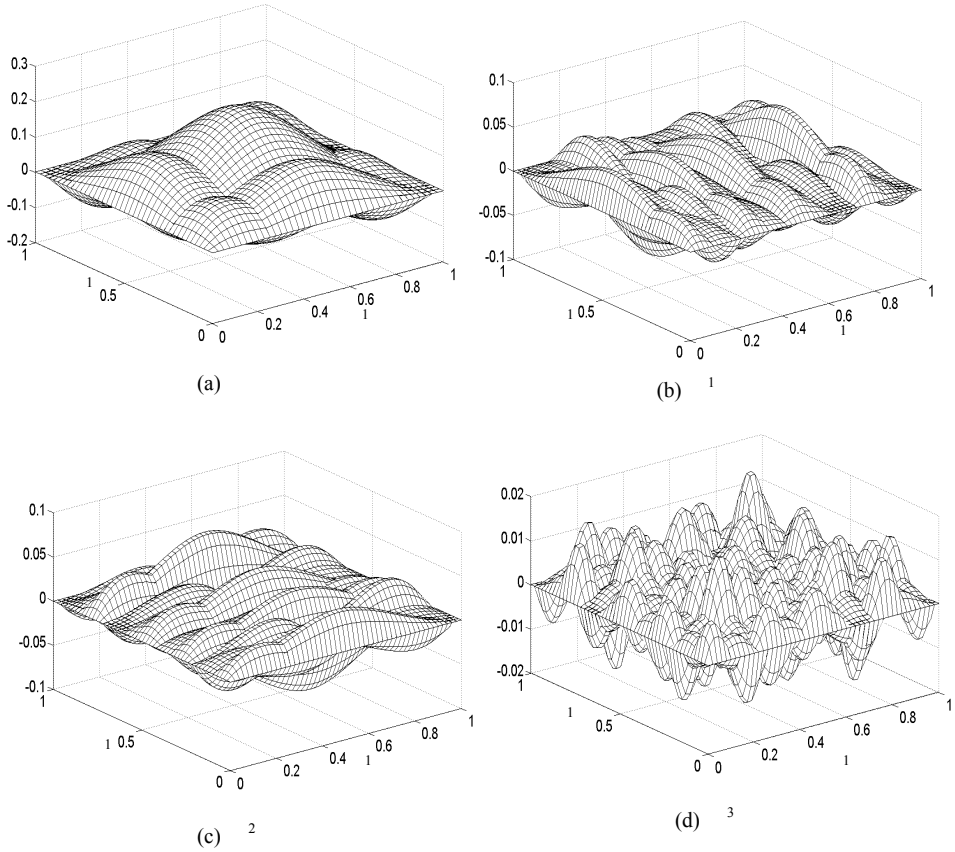

Figure 4: Two-dimensional HCSWI scaling functions $\boldsymbol{\phi}^1$ and wavelets $\boldsymbol{\psi}^1$, $\boldsymbol{\psi}^2$ and $\boldsymbol{\psi}^3$

3 Numerical computation formulas using HCSWI

Plane elasticity includes plane stress and plane strain problems. Here, the plane stress problem is analyzed and the plane strain problem is similarly if Young's

modulus E and Poisson's ratio μ are replaced by $E/(1-\mu^2)$ and $\mu/(1-\mu)$ respectively. The generalized function of potential energy for plane stress problem is [Zienkiewicz, O.C., Taylor, R.L. (2000)]

$$\mathbf{\Pi}_p(\boldsymbol{\delta}) = \int_{\Omega} \frac{1}{2}\boldsymbol{\varepsilon}^{\mathrm{T}}\mathbf{D}\boldsymbol{\varepsilon} t dxdy - \int_{\Omega} \boldsymbol{\delta}^{\mathrm{T}}\mathbf{f} t dxdy - \int_{S_\sigma} \boldsymbol{\delta}^{\mathrm{T}}\mathbf{p} t ds - \sum_{i=1}^{n} \boldsymbol{\delta}_i^{\mathrm{T}}\mathbf{F}_i \tag{8}$$

where Ω is the solving domain with length l_x and l_y,t is the plate thickness, $\mathbf{f} = \{f_x\ f_y\}^{\mathrm{T}}$ are the body forces, $\boldsymbol{\delta} = \{u\ v\}^{\mathrm{T}}$ are the displacements, $\mathbf{p} = \{p_x\ p_y\}^{\mathrm{T}}$ are the surface forces, $\mathbf{F}_i = \{F_{xi}\ F_{yi}\}^{\mathrm{T}}$ are point forces, $\boldsymbol{\delta}_i = \{u_i\ v_i\}^{\mathrm{T}}$ are the point displacements, $\mathbf{D}$ is the elastic matrix, and $\boldsymbol{\varepsilon} = \{\varepsilon_x\ \varepsilon_y\ \gamma_{xy}\}^{\mathrm{T}}$ are the strain components. $\mathbf{D}$ and $\boldsymbol{\varepsilon}$ are given by

$$\mathbf{D} = \frac{E}{1-\mu^2}\begin{bmatrix} 1 & \mu & 0 \\ \mu & 1 & 0 \\ 0 & 0 & \frac{1-\mu}{2} \end{bmatrix}$$

and

$$\boldsymbol{\varepsilon} = \begin{bmatrix} \frac{\partial}{\partial x} & 0 \\ 0 & \frac{\partial}{\partial y} \\ \frac{\partial}{\partial y} & \frac{\partial}{\partial x} \end{bmatrix} \mathbf{u} \tag{9}$$

The relationship between stress and strain is

$$\boldsymbol{\sigma} = \{\sigma_x\ \sigma_y\ \tau_{xy}\}^T = \mathbf{D}\varepsilon \tag{10}$$

The two-dimensional HCSWI bases are employed as interpolating functions to construct multi-scale approximation equations as

$$u = \boldsymbol{\phi}_j^{\mathrm{T}}\mathbf{u}$$

and

$$v = \boldsymbol{\phi}_j^{\mathrm{T}}\mathbf{v} \tag{11}$$

where

$$\begin{cases} \mathbf{u} = \{u_1 \dots u_{2^{j+1}} | \cdots | u_{2^{j+2}-2^{j+1}+1} \dots u_{2^{j+1}}\}^{\mathrm{T}} \\ \mathbf{v} = \{v_1 \dots v_{2^{j+1}} | \cdots | v_{2^{j+2}-2^{j+1}+1} \dots v_{2^{j+1}}\}^{\mathrm{T}} \end{cases} \tag{12}$$

are the column vectors of wavelet interpolating coefficients (also the DOFs) to be determined.

Substituting Eqs. (9-11) into Eq.(8) and let $\delta\mathbf{\Pi}_p = 0$, we have

$$\begin{bmatrix} \mathbf{K}^1 & \mathbf{K}^2 \\ \mathbf{K}^3 & \mathbf{K}^4 \end{bmatrix} \begin{bmatrix} \mathbf{u} \\ \mathbf{v} \end{bmatrix} = \begin{bmatrix} \mathbf{P}_a \\ \mathbf{P}_b \end{bmatrix} \tag{13}$$

where

$$\mathbf{P}_a = \int_{S_\sigma} p_x \boldsymbol{\phi}_j^{\mathrm{T}} \mathrm{d}s + \int_{\Omega} f_x \boldsymbol{\phi}_j^{\mathrm{T}} \mathrm{d}\Omega + \sum_{i=1}^{n} \boldsymbol{\phi}_j^{\mathrm{T}}(\xi_i, \eta_i) F_{ix}\} \tag{14}$$

$$\mathbf{P}_b = \int_{S_\sigma} p_y \boldsymbol{\phi}_j^{\mathrm{T}} \mathrm{d}s + \int_{\Omega} f_y \boldsymbol{\phi}_j^{\mathrm{T}} \mathrm{d}\Omega + \sum_{i=1}^{n} \boldsymbol{\phi}_j^{\mathrm{T}}(\xi_i, \eta_i) F_{iy} \tag{15}$$

$$\mathbf{K}^1 = E/(1-\mu^2)(\mathbf{A}_1^{11} \otimes \mathbf{A}_2^{00} + (1-\mu)/2\mathbf{A}_1^{00} \otimes \mathbf{A}_2^{11}) \tag{16}$$

$$\mathbf{K}^2 = E/(1-\mu^2)(\mu\mathbf{A}_1^{10} \otimes \mathbf{A}_2^{01} + (1-\mu)/2\mathbf{A}_1^{01} \otimes \mathbf{A}_2^{10}) \tag{17}$$

$$\mathbf{K}^3 = (\mathbf{K}^2)^{\mathrm{T}} \tag{18}$$

$$\mathbf{K}^4 = E/(1-\mu^2)(\mathbf{A}_1^{00} \otimes \mathbf{A}_2^{11} + (1-\mu)/2\mathbf{A}_1^{11} \otimes \mathbf{A}_2^{00}) \tag{19}$$

in which

$$\mathbf{A}_1^{00} = l_x \int_0^1 \boldsymbol{\phi}_j^{\mathrm{T}} \boldsymbol{\phi}_j \mathrm{d}\xi \tag{20}$$

$$\mathbf{A}_1^{01} = \int_0^1 \boldsymbol{\phi}_j^{\mathrm{T}} \frac{\mathrm{d}\boldsymbol{\phi}_j}{\mathrm{d}\xi} \mathrm{d}\xi \tag{21}$$

$$\mathbf{A}_1^{10} = (\mathbf{A}_1^{01})^{\mathrm{T}} \tag{22}$$

$$\mathbf{A}_1^{11} = 1/l_x \int_0^1 \frac{\mathrm{d}\boldsymbol{\phi}_j^{\mathrm{T}}}{\mathrm{d}\xi} \frac{\mathrm{d}\boldsymbol{\phi}_j}{\mathrm{d}\xi} \mathrm{d}\xi \tag{23}$$

$\mathbf{A}_2^{lm}(l, m = 0, 1)$ is similarly to $\mathbf{A}_1^{lm}(l, m = 0, 1)$ when l_x and $\mathrm{d}\xi$ are replaced by l_y and $\mathrm{d}\eta$ respectively.

The lifting scheme for multi-scale calculating SIFs is similar to Ref.[Xiang et al. (2009b)]. Fig.5 shows the lifting scheme to lift the scale from 1 to j.

When the scale 1 is lifted to scale j, $\mathbf{A}_1^{11}$ and $\mathbf{A}_2^{11}$ would be decomposed totally across different scale. The integral $\mathbf{A}_1^{11}$ is

$$\mathbf{A}_1^{11} = 1/l_x \begin{bmatrix} \int_0^1 \frac{\mathrm{d}\boldsymbol{\phi}_1^{\mathrm{T}}}{\mathrm{d}\xi} \frac{\mathrm{d}\boldsymbol{\phi}_1}{\mathrm{d}\xi} \mathrm{d}\xi & \mathbf{0} & \cdots & \mathbf{0} \\ & \int_0^1 \frac{\mathrm{d}\boldsymbol{\psi}_1^{\mathrm{T}}}{\mathrm{d}\xi} \frac{\mathrm{d}\boldsymbol{\psi}_1}{\mathrm{d}\xi} \mathrm{d}\xi & \cdots & \mathbf{0} \\ \text{symmetry} & & \ddots & \vdots \\ & & & \int_0^1 \frac{\mathrm{d}\boldsymbol{\psi}_{j-1}^{\mathrm{T}}}{\mathrm{d}\xi} \frac{\mathrm{d}\boldsymbol{\psi}_{j-1}}{\mathrm{d}\xi} \mathrm{d}\xi \end{bmatrix} \tag{24}$$

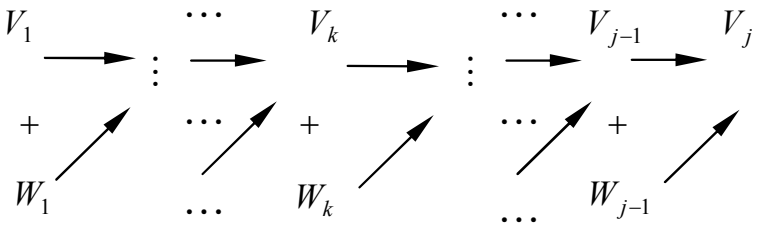

Figure 5: The lifting scheme of wavelet bases

The integrals $\mathbf{A}_1^{01}$, $\mathbf{A}_2^{01}$, $\mathbf{A}_1^{00}$ and $\mathbf{A}_2^{00}$ would be preserved coupling relationship. However, the former generated sub-matrices need not be re-calculated. This property can also increase the calculating efficiency. The integral $\mathbf{A}_1^{01}$ is

$$\mathbf{A}_1^{01} = \begin{bmatrix} \int_0^1 \boldsymbol{\phi}_1^{\mathrm{T}} \frac{\mathrm{d}\boldsymbol{\phi}_1}{\mathrm{d}\xi}\mathrm{d}\xi & \int_0^1 \boldsymbol{\phi}_1^{\mathrm{T}} \frac{\mathrm{d}\boldsymbol{\psi}_1}{\mathrm{d}\xi}\mathrm{d}\xi & \cdots & \int_0^1 \boldsymbol{\phi}_1^{\mathrm{T}} \frac{\mathrm{d}\boldsymbol{\psi}_{j-1}}{\mathrm{d}\xi}\mathrm{d}\xi \\ & \int_0^1 \boldsymbol{\psi}_1^{\mathrm{T}} \frac{\mathrm{d}\boldsymbol{\psi}_1}{\mathrm{d}\xi}\mathrm{d}\xi & \cdots & \int_0^1 \boldsymbol{\psi}_1^{\mathrm{T}} \frac{\mathrm{d}\boldsymbol{\psi}_{j-1}}{\mathrm{d}\xi}\mathrm{d}\xi \\ \text{symmetry} & & \ddots & \vdots \\ & & & \int_0^1 \boldsymbol{\phi}_{j-1}^{\mathrm{T}} \frac{\mathrm{d}\boldsymbol{\psi}_{j-1}}{\mathrm{d}\xi}\mathrm{d}\xi \end{bmatrix} \tag{25}$$

and the integral $\mathbf{A}_1^{00}$ is

$$\mathbf{A}_1^{00} = l_x \begin{bmatrix} \int_0^1 \boldsymbol{\phi}_1^{\mathrm{T}} \boldsymbol{\phi}_1 \mathrm{d}\xi & \int_0^1 \boldsymbol{\phi}_1^{\mathrm{T}} \boldsymbol{\psi}_1 \mathrm{d}\xi & \cdots & \int_0^1 \boldsymbol{\phi}_1^{\mathrm{T}} \boldsymbol{\psi}_{j-1} \mathrm{d}\xi \\ & \int_0^1 \boldsymbol{\psi}_1^{\mathrm{T}} \boldsymbol{\phi}_1 \mathrm{d}\xi & \cdots & \int_0^1 \boldsymbol{\psi}_1^{\mathrm{T}} \boldsymbol{\psi}_{j-1} \mathrm{d}\xi \\ \text{symmetry} & & \ddots & \vdots \\ & & & \int_0^1 \boldsymbol{\phi}_{j-1}^{\mathrm{T}} \boldsymbol{\psi}_{j-1} \mathrm{d}\xi \end{bmatrix} \tag{26}$$

4 Numerical investigations

In this study, the displacement extrapolation technique has been used to calculate the SIFs as follows [Tada et al. (2000)]

$$v = \frac{K_I}{2G}\sqrt{\frac{r}{2\pi}}(k+1) \tag{27}$$

where r is the distance from crack tip to a point considered along with the crack edge, $k = (3-\mu)/(1+\mu)$ is the elastic parameter, $G = \frac{E}{2(1+\mu)}$ is shear modulus. Therefore, we obtain SIFs for crack with mode I as

$$K_I = \frac{2Gv}{(k+1)}\sqrt{\frac{2\pi}{r}} \tag{28}$$

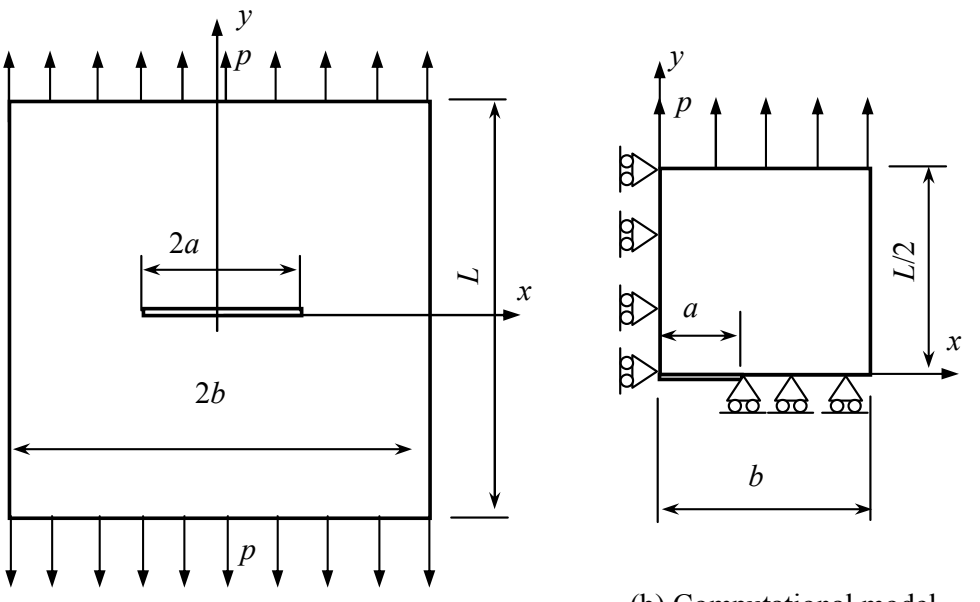

(a) The center crack (b) Computational model

Figure 6: The center crack problem and numerically computational model

4.1 Example 1: The center crack problem

The central cracked plate and the computational model are shown in Fig.6(a) and(b) respectively. The geometry is imposed by a plane stress condition with symmetrical uniform load p applied under mode I loading condition. Plate length is $2b$, width L and centre crack width is $2a$. The analytical SIFs for this problem is given by Ref. [Tada et al. (2000)] as

$$K_I = p\sqrt{\pi a}F(a/b) \tag{29}$$

To make a simple comparison, the non-dimensional stress intensity factor is defined as follows

$$Z_I = \frac{K_I}{p\sqrt{a}} \tag{30}$$

Error estimate is necessary to make an adaptive wavelet numerical calculation. If the SIFs of wavelet numerical solution Z_I^{i+1} and Z_I^i (i+1 and i denote the neighbor scales) is chosen as the benchmark, with the defined dimensionless relative error (error estimate) as the following equation

$$\varepsilon^* = \left|Z^{i+1} - Z^i\right| / Z^{i+1} \tag{31}$$

Given the error threshold ε_0^*, error estimate ε^* can be made according to Eq. (31). When an error ε^* in a certain scale is large than the error threshold ε_0^*, i.e., $\varepsilon^* > \varepsilon_0^*$, scale will be lifted to the higher one. This process will be repeated until solution is less than error threshold ε_0^*. Therefore, the adaptive analysis algorithm is listed below:

(1) Give the error threshold ε_0^*

(2) Use scaling functions scale $\boldsymbol{\phi}_i$ and $\boldsymbol{\Phi}_{i+1}$ to calculate the corresponding Z^i and Z^{i+1}, respectively.

(3) Calculate error estimate ε^* according to Eq. (29).

(4) Compare ε^* and ε_0^*, if $\varepsilon_i^* > \varepsilon_0^*$, then go back to step (2). Otherwise, stop the calculation and obtain the results.

Suppose the error threshold $\varepsilon_0^* = 0.01$, it found that only three interactions were performed to obtain a comfortable result at scale j=4, as shown in Table 1. Different methods are used to make a comparison, such as:

Method 1: Analytical solution, the value of $F(a/b)$ is shown in Ref.[Tada et al. (2000)].

Method 2: Analytical solution, the other value of $F(a/b)$ is calculated by [Tada et al. (2000)]

$$F(a/b) = \{1 - 0.025(\frac{a}{b})^2 + 0.06(\frac{a}{b})^4\}\sqrt{\sec\frac{\pi a}{2b}} \tag{32}$$

Method 3: Adaptive finite element method with about 5000 DOFs as shown in Ref. [Souiyah et al. (2009)].

Present method: The present results computed using HCSWI bases at level j=4. It notes that the DOFs of multi-scale approximation equation at each scale j=1, 2, 3, 4 are 32, 128, 512 and 2048, respectively.

The present results computed using HCSWI bases at level j=4 are found to be in good agreement with those in literature, as shown in Table 1. By comparing with other methods, the relative errors to the analysis solution is less than 0.261% for all values, which gives highly accurate results and much better than 2.195% of adaptive finite element method with about 5000 DOFs. In order to show the performance of the present method, we give a comparison of the computational cost of the present method with finite element method. All the computations are conducted using Matlab2010a on a laptop computer with a 2 GHz dual-core CPU (T4200) and 2GB memory. According to the TIC and TOC commands of Matlab2010a, the computing times required to Method 3 is about 4.5 seconds, whereas the present method is less than 3 seconds (only measured time for the level j=4). Moreover, the DOFs of adaptive finite element method are almost 2.5 times of those of the present method. Therefore, the performance of the present wavelet-based numeri-

Table 1: Stress intensity factors Z_I for different a/b ($L/2b$=1) for exmaple 1

a/b	Method 1		Method 2			Method 3			Present method	
	$F(a/b)$	Z_I	$F(a/b)$	Z_I	Error/%	$F(a/b)$	Z_I	Error/%	Z_I^4	Error/%
0.1	1.006	1.7831	1.006	1.783	0.006	1.001	1.7742	0.499	1.7833	0.011
0.2	1.0246	1.8161	1.0245	1.8158	0.017	1.0237	1.8145	0.088	1.8148	0.072
0.3	1.0557	1.8747	1.0575	1.8744	0.016	1.0416	1.8462	1.520	1.8698	0.261
0.4	1.1094	1.9664	1.109	1.9657	0.036	1.109	1.9657	0.036	1.9655	0.046
0.5	1.1867	2.1034	1.1862	2.1025	0.043	1.1879	2.1055	0.100	2.1031	0.014
0.6	1.3033	2.31	1.3028	2.3091	0.039	1.2747	2.2593	2.195	2.311	0.043
0.7	1.4882	2.6378	1.4874	2.6363	0.057	1.4655	2.5975	1.528	2.6352	0.099
0.8	1.816	3.2188	1.8143	3.2158	0.093	1.8131	3.2136	0.162	3.2253	0.202
0.9	2.5776	4.5687	2.5767	4.567	0.037	2.565	4.5463	0.490	4.5608	0.173

cal is verified and the good performance of the lifting scheme is observed when the wavelets are added step by step to realize multi-scale approximation of SIFs.

The SIFs Z_I^1, Z_I^2 and Z_I^3 and the corresponding ε^* of HCSWI wavelet bases at scale j=1, 2, 3 are listed in Table 2.

Table 2: Stress intensity factors Z_I^i (i=1,2,3) for different a/b ($L/2b$=1)

a/b	Z_I^1	ε^*	Z_I^2	ε^*	Z_I^3	ε^*
0.1	1.5821	0.058	1.6793	0.050	1.7685	0.008
0.2	1.6944	0.022	1.7319	0.013	1.7555	0.033
0.3	1.8020	0.017	1.8326	0.022	1.8736	0.002
0.4	2.1053	0.047	2.0117	0.013	1.9854	0.010
0.5	2.2261	0.016	2.1910	0.031	2.1245	0.010
0.6	2.4758	0.024	2.4189	0.037	2.3327	0.009
0.7	2.7845	0.032	2.6980	0.028	2.6246	0.004
0.8	3.3725	0.015	3.3212	0.022	3.2488	0.007
0.9	4.4287	0.015	4.4956	0.011	4.5463	0.003

4.2 Example 2: The double edge crack problem

Figure 7 shows a double edge cracked plate and its computational model. We compare the present method using HCSWI bases at level j=4 with traditional finite element method (PLANE42 element in software ANSYS) with 200×200meshes (80000 DOFs). The benchmark to compare the two methods is the analytical solution given by [Tada et al. (2000)]

$$F(a/b) = \frac{1.122 - 0.561(\frac{a}{b}) - 0.205(\frac{a}{b})^2 + 0.471(\frac{a}{b})^3 - 0.190(\frac{a}{b})^4}{\sqrt{1-a/b}} \tag{33}$$

Table 3 shows the relative errors between the two methods and the analytical solutions. The relative errors between results of the proposed method and the analytical solutions are less than 1.763% for all a/b, which are much smaller than that (5.926%) obtained using the traditional finite element method (PLANE42 element in software ANSYS) with 80000 DOFs.

By summarizing the above SIFs analysis and comparisons, the validity of the present method is testified.

5 Conclusions

Properties of wavelet of good localization are used to approximate displacement fields near the crack tip. Wavelet-based numerical method to analyze plate struc-

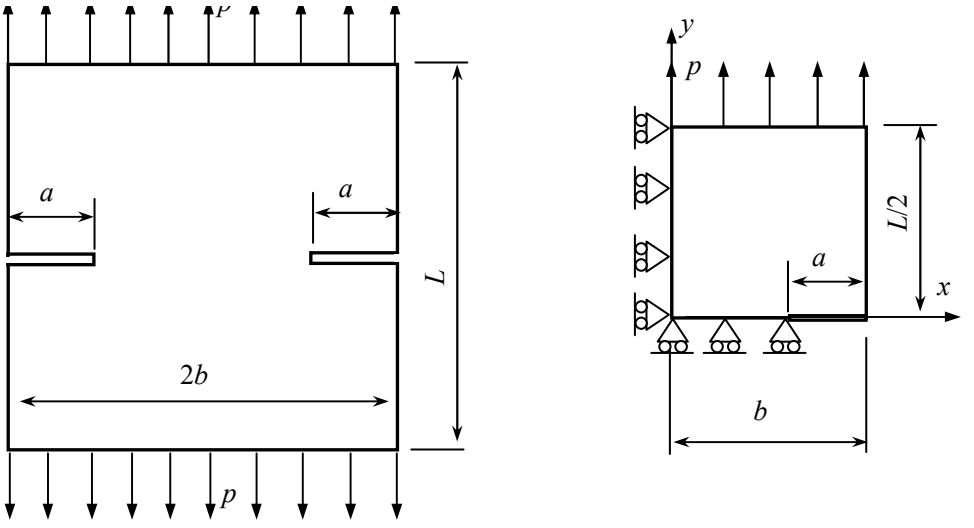

(a) The double edge crack (b) Computational Model

Figure 7: The double-edge cracked plate and its computational model

Table 3: Stress intensity factors Z_I for different a/b under uniform tension ($L/2b$=1) for exmaple 2

a/b	Analytical solution [Tada et al. (2000)]		PLANE42		Proposed method	
	$F(a/b)$	Z_I	Z_I	Error/%	Z_I	Error/%
0.1	1.1219	1.9885	1.8860	5.437	1.9785	0.503
0.2	1.1237	1.9917	1.9633	1.446	1.9856	0.306
0.3	1.1312	2.005	2.0552	2.443	2.0212	0.808
0.4	1.1491	2.0367	2.1471	5.143	2.0726	1.763
0.5	1.1841	2.0987	2.2309	5.926	2.105	0.300
0.6	1.2471	2.2104	2.3181	4.646	2.245	1.565
0.7	1.3598	2.4102	2.4528	1.736	2.3875	0.942
0.8	1.5771	2.7954	2.7416	1.961	2.7784	0.608
0.9	2.1179	3.7539	3.5608	5.424	3.6932	1.617

tures using HCSWI bases is established to simulate singularity problems. For the good characteristics of the wavelet bases of HCSWI, such as multi-resolution analysis and orthogonal according to the inner product of $\langle u', v' \rangle$, the lifting scheme of the present method can be realized efficiently. Therefore, the present method has at least two advantages. The first advantage is that the computation efficiency,

necessary for achieving a solution with the same accuracy compared with the usual finite element method, are much reduced. The second advantage stems from the fact that the so-called multi-resolutions of wavelets make it possible to generate a multi-scale approximation equation for the singularity problems. For the orthogonal characteristic of the wavelet bases with respect to the given inner product, the corresponding multi-scale equations will be decoupled across scales partially and suit for nesting approximation. The numerical results show that wavelet numerical method is suitable to compute SIFs for plate structures.

Acknowledgement: Authors are gratefully acknowledging the financial support by the projects of National Natural Science Foundation of China (Nos.51175097, 51105085, 51165003). This work is also supported funded by Zhejiang Technologies R&D Program of China (No. 2010C31094) and Zhejiang Provincial Natural Science Foundation of China under Grant No.Y1110046.

References

Chen, X.F., Yang, S.J., Ma, J.X., He, Z.J. (2004): The construction of wavelet finite element and its application, *Finite Elem. Anal. Des.* 40, 541-554.

Chen, X.F., Li, B., Xiang, J.W., He, Z.J. (2009): Quantitative identification of rotor cracks based on finite element of B-spline wavelet on the interval. *Int. J. Wavelets Multiresolut. Inf. Processing*. 7, 443-457.

Diaz, L.A., Martin, M.T., Vampa, V. (2009): Daubechies wavelet beam and plate finite elements. *Finite Elem. Anal. Des.* 45, 200-209.

Giner, E., Sukumar, N., Tarancón, J.E. et al. (2009): An Abaqus implementation of the Extended Finite Element Method, *Eng. Fract. Mech.* 76, 347-368.

He, Y.M., Chen, X.F., J.W. Xiang, He, Z.J. (2007): Adaptive multiresolution finite element method based on second generation wavelets , *Finite Elem. Anal. Des.* 43, 566-579.

Jia, R.Q. , Liu, S.T. (2006): Wavelet bases of Hermite cubic splines on the interval, *Adv. Comput. Math* 25, 23-39.

Jia, R.Q. (2009): Spline wavelets on the interval with homogeneous boundary conditions, *Adv. Comput. Math* 30, 177-200.

Kpegba, K.W., Ottavy, N. (1996): Stress intensity factors in two-dimensional crack problems by using the Superimposed Meshes Method. *Eng. Fract. Mech.*54, 113-125.

Ma, J.X., Xue, J.J., Yang, S.J., He, Z.J. (2003): A study of the construction and application of a Daubechies wavelet-based beam element, *Finite Elem. Anal. Des.* 39, 965-975.

Mallat, S. (1999): *A Wavelet Tour of Signal Processing*, Academic Press, London.

Souiyah, M., Alshoaibi, A., Muchtar, A. et al. (2009): Two-dimensional finite element method for stress intensity factor using adaptive mesh strategy, *Acta. Mech.* 204, 99-108.

Tada, H., Paris, P.C., Irwin, G.R. (2000): *The Stress Analysis of Cracks Handbook*, ASME Press, New York.

Vampa, V., Martin, M.T., Serrano, E. (2010): A hybrid method using wavelets for the numerical solution of boundary value problems on the interval. *Appl. Math. Comput.* 217, 3355-3367.

Wang, Y.M.,, Chen, X.F.,, He, Z.J. (2010): Adaptive multiwavelet-hierarchical method for multiscale computation, *Int. J. Multiscale Comput. Eng.* 8, 397-409.

Wang, Y.M.,, Chen, X.F.,, He, Z.J. (2011): The construction of finite element multiwavelets for adaptive structural analysis, *Int. J. Numer. Method Bio. Eng.* 27, 562-584.

Wearing, J. L., Ahmadi-Brooghani, S.Y. (1999): The evaluation of stress intensity factors in plate bending problems using the dual boundary element method, *Eng. Anal. Bound. Elem.* 23, 3-19.

Xiang, J.W., Chen, X.F., Mo, Q.Y., He, Z.J. (2007): Identification of Crack in a Rotor System Based on Wavelet Finite Element Method, *Finite Elem. Anal. Des.* 43, 1068-1081.

Xiang, J.W., Chen, D.D., Chen, X.F.,, He, Z.J. (2009a): A novel wavelet-based finite element method for the analysis of rotor-bearing systems, *Finite Elem. Anal. Des.* 45, 908-916.

Xiang, J.W., Chen, X.F., Li, X.K. (2009b): Numerical solution of Possion equation by using wavelet bases of Hermite cubic splines on the interval, *Appl. Math. Mech.-Engl. Ed.* 30, 1325-1334.

Zhang, X.W., Chen, X.F., Wang, X.Z., He, Z.J. (2010): Multivariable finite elements based on B-spline wavelet on the interval for thin plate static and vibration analysis, *Finite Elem. Anal. Des.* 46, 416-427.

Zienkiewicz, O.C., Taylor, R.L. (2000): *Finite Element Method*, Volume 1 - The Basis,5th Ed., Academic Press, London.